

Wind structure of late B supergiants.

I. Multi-line analyses of near-surface and wind structure in HD 199 478 (B8 Iae).

N. Markova¹, R. K. Prinja², H. Markov¹, I. Kolka³, N. Morrison⁴, J. Percy⁵, S. Adelman⁶

¹ Institute of Astronomy, National Astronomical Observatory, Bulgarian Academy of Sciences, P.O. Box 136, 4700 Smoljan, Bulgaria
e-mail: nmarkova@astro.bas.bg, hmarkov@astro.bas.bg

² Department of Physics & Astronomy, UCL, Gower Street, London WC1E 6BT, UK
e-mail: rkp@star.ac.uk

³ Tartu Observatory, Toravere 61602, Estonia
e-mail: indrek@aai.ee

⁴ Ritter Observatory, The University of Toledo, Toledo, OH 43606, USA
e-mail: NMORRIS2@uoft02.utoledo.edu

⁵ Department of Astronomy and Astrophysics, University of Toronto, Toronto ON Canada, M5S 3H4
e-mail: jpercy@utm.utoronto.ca

⁶ Department of Physics, The Citadel, Charleston SC 29409-0270, USA
e-mail: adelmans@citadel.edu

Received; accepted

ABSTRACT

Aims. We provide a quantitative analysis of time-variable phenomena in the photospheric, near-star, and outflow regions of the late-B supergiant (SG) HD 199 478. This study aims to provide new perspectives on the nature of outflows in late-B SGs and on the influence of large-scale structures rooted at the stellar surface.

Methods. The analysis is based primarily on optical spectroscopic datasets secured between 1999 and 2000 from the Bulgarian NAO, Tartu, and Ritter Observatories. The acquired time-series samples a wide range of weak metal lines, He I absorption, and both emission and absorption signatures in H α . Non-LTE line synthesis modelling is conducted using FASTWIND for a strategic set of late-B SGs to constrain and compare their fundamental parameters within the context of extreme behaviour in the H α lines.

Results. The temporal behaviour of HD 199 478 is characterised by three key empirical properties: (i) systematic central velocity shifts in the photospheric absorption lines, including C II and He I, over a characteristic time-scale of ~ 20 days; (ii) extremely strong, variable H α emission with no clear modulation signal, and (iii) the occurrence in 2000 of a (rare) high-velocity absorption (HVA) event in H α , which evolved over ~ 60 days, showing the clear signature of mass infall and outflows. In these properties HD 199 478 resembles few other late-B SGs with peculiar emission and HVAs in H α (HD 91 619, HD 34 085, HD 96919). Different possibilities accounting for the phenomenon observed are indicated and briefly discussed.

Conclusions. At the cooler temperature edge of B SGs, there are objects whose wind properties, as traced by H α , are inconsistent with the predictions of the smooth, spherically symmetric wind approximation. This discordance is still not fully understood and may highlight the role of a non-spherical, disk-like, geometry, which may result from magnetically-driven equatorial compression of the gas. Ordered dipole magnetic fields may also lead to confined plasma held above the stellar surface, which ultimately gives rise to transient HVA events.

Key words. stars: early-type – stars: SGs – stars: fundamental parameters – stars: winds, outflows – stars: magnetic fields – stars: individual: HD 199 478

1. Introduction

The key limiting assumptions incorporated within current hot star model atmospheres include a globally stationary and spherically symmetric stellar wind with a smooth density stratification. Although these models are generally quite successful in

describing the overall wind properties, there are numerous observational and theoretical studies which indicate that hot star winds are certainly not smooth and stationary. Most (if not all) of the time-dependent constraints refer, however, to O-stars and early B supergiants (SGs), while mid- and late-B candidates are currently under-represented in the sample of stars investigated to date.

Vink et al. (2000) have shown that for mid and late-B SGs there is a discrepancy between theoretical predictions and $H\alpha$ mass-loss rates, derived by means of unblanketed model analysis. This finding was confirmed by recent investigations using line-blanketed model atmospheres (see, e.g., Crowther et al. 2006; Markova & Puls 2008). The reason for the discrepancies is not clear yet but wind structure and variability might in principle cause them. Indeed, observations indicate that while winds in late-B SGs are significantly weaker than those in O SGs (e.g. Markova & Puls 2008), there is no currently established reason to believe that weaker winds might be less structured/variable than stronger ones (e.g. Markova et al. 2005; Puls et al. 2006).

The first extended spectroscopic monitoring campaigns of line-profile variability (lpv) in late-B SGs were performed by Kaufer et al. (1996a,b), who showed that stellar winds at the cooler temperature edge of the B-stars domain can also be highly variable. Interestingly, in all 3 cases studied by these authors, the variability patterns (as traced by $H\alpha$) were quite similar consisting of (i) blue- and red-shifted emission with V/R variations similar to those in Be-stars, and (ii) the sudden appearance of deep and highly blue-shifted absorptions (HVAs). Though the kinematic properties of the HVAs in $H\alpha$ were found to be completely different from those of DACs (Discrete Absorption Components) in the UV spectra of O and early-B stars (e.g., HVAs do not propagate outwards, but instead extend to zero velocity and even indicate mass infall), similar scenarios consisting of large-scale wind structures rooted in the photosphere were suggested to interpret their appearance and development in time.

The present paper is focused on a multi-line investigation of HD 199 478 (HR 8020), a B8 Iae star whose stellar and wind properties have been recently determined by means of NLTE model atmosphere analysis of strategic lines in the optical (Markova & Puls 2008). The first extensive monitoring campaign of lpv in the optical spectrum of this star revealed $H\alpha$ variability similar to those described by Kaufer et al. (i.e., peculiar wind emission with V/R variations similar to those in Be stars) with one exception, i.e. no indications for any HVAs were found during that survey (Markova & Valchev 2000). In addition to wind variability significant absorption lpv was also established, which raised suggestions of a link stellar pulsations. To check the pulsational hypothesis however long-term photometric observations were required.

Motivated by the intriguing time-variable properties reported above, we organised and conducted new parallel spectroscopic and photometric monitoring campaigns of HD 199 478 during 1999 and 2000. Details of the spectroscopic analysis are presented here and the results of the photometric survey were recently published by (Percy et al. 2008).

2. Observations and data reduction

2.1. Spectral data

Spectroscopic data consisting of 65 spectra centered on $H\alpha$ and 46 on He I $\lambda 5876$ were predominantly collected at the National Astronomical Observatory (NAO), Bulgaria while individual

$H\alpha$ observations were also secured at the Tartu Observatory (TO), Estonia and at Ritter Observatory (RO), USA.

The total time coverage of these data is from January 1999 to December 2000 with large data gaps in the summer and the winter each year. The time sampling was typically 3 to 6 spectra per month with a time-interval between successful exposures of 1 to 2 days, except for the fall of 2000 when HD 199 478 was monitored more intensively. The time distribution of the data and spectral regions observed are given in Table 2 while specific information about the equipment, reduction strategy and methods used at each observatory is outlined below and summarised in Table 1.

National Astronomical Observatory, Smolyan, Bulgaria – A total of 95 high-quality spectra (49 in $H\alpha$ and 46 in He I $\lambda 5876$) were obtained (observers T. Valchev and H. Markov) in the coudé focus of the NAO 2m telescope of the Bulgarian Academy of Sciences during the period March, 1999 – December, 2000. Most of the observations (91) were carried out using a BL632/14.7 grooves mm^{-1} grating in first order together with a PHOTOMETRICS CCD (1024 x 1024, 24μ) as a detector¹. This configuration produces spectra with a reciprocal dispersion of $\sim 0.2 \text{ \AA pixel}^{-1}$ and an effective resolution of ~ 2.0 pixels ($\sim 0.44 \text{ \AA R}=15\,000$) over a wavelength range of $\sim 204 \text{ \AA}$. In addition, four more $H\alpha$ spectra with a reciprocal dispersion of $\sim 0.1 \text{ \AA pixel}^{-1}$ and an effective resolution of ~ 2.0 pixels ($\sim 0.2 \text{ \AA R}=30\,000$) were obtained using a BL632/22.3 grooves mm^{-1} grating in second order and the same detector. The S/N ratios of the NAO spectra range between 250 and 450.

We followed a standard procedure for data reduction (developed in IDL) including: bias subtraction, flat-fielding, cosmic ray removal, wavelength calibration, correction for heliocentric radial velocity ($V_r = -12 \text{ km s}^{-1}$), water vapour line removal and rebinning to a step of 0.2 \AA per pixel. More information about the reduction procedure can be found elsewhere (Markova & Valchev 2000; Markova et al. 2004).

Tartu Observatory, Toravere, Estonia – At TO (observer I. Kolka) 9 $H\alpha$ spectra were obtained using a 1.5-m reflector equipped with a Cassegrain spectrograph and an Orbis-1 (LN2-cooled) CCD camera (512x512 pixels). About 130 \AA is covered by one exposure with a reciprocal dispersion of 0.25 \AA/pix resulting in a resolution of about 16 000 at $H\alpha$.

The observations were reduced in a uniform way using MIDAS. Due to the very low dark current, the mean background subtracted from the raw frames is a sum of bias plus dark and real sky. Flat-fielding was not performed due to the reasonably flat response of the CCD and to the empirical result that the spectrum summed over 4 - 6 CCD rows has almost no distortion from pixel to pixel sensitivity differences. Thus, the photon noise and the read-out noise are the main sources of errors. The telluric water vapour lines were removed by dividing individual spectra with a scaled model telluric spectrum.

¹ This detector was characterised by a *rms* read-out noise 3.3 electrons per pixel (2.7 ADU with 1.21 electrons per ADU)

Table 1. Spectral observations and instruments employed.

Observatory	Telescope	Instrument	$R=\lambda/\delta\lambda$	window [in Å]	region	N_{spec}	
National Astron. Obs.	NAO	2.0m	coudé	15 000	204	H α	45
National Astron. Obs.	NAO	2.0m	coudé	30 000	100	H α	4
National Astron. Obs.	NAO	2.0m	coudé	15 000	204	He I λ 5876	46
Tartu Observatory	TO	1.5m	long-slit	16 000	127	H α	9
Ritter Observatory	RO	1.1m	fiber-fed	26 000	70	H α	7

Table 2. Summary of the spectral data sets.

Region	Observational dates	HJD 2451200+	N_{spec}	S/N
H α + CII	1998 Dec.,30 – May, 2	40.6 – 101.6	8	240
H α + CII	1999 Sept.,17 – Dec., 2	239.4 – 315.2	15	423
H α + CII	2000 March, 28 – June, 23	432.6 – 519.4	10	275
H α + CII	2000 Sept, 5 – Dec., 8	592.7 – 687.2	32	320
He I λ 5876	1999 March, 2 – April, 24	40.6 – 93.5	4	240
He I λ 5876	1999 Sept, 17 – Dec., 2	239.4 – 315.2	15	423
He I λ 5876	2000 March, 28 – June, 23	432.6 – 519.4	10	275
He I λ 5876	2000 Sept., 14 – Dec., 8	602.3 – 687.2	17	320

Finally, the spectra were corrected to the stellar rest frame for a radial velocity of -12 km s^{-1} and normalised to the continuum.

Ritter Observatory, Toledo, USA – The Ritter spectra were obtained with a 1-m telescope, fiber-fed échelle spectrograph, and Wright Instruments CCD camera at the University of Toledo over a period of two months (September – November) in 2000. The spectral resolving power $R \approx 26\,000$, with the resolution element having a FWHM of about 4 pixels. The spectral coverage consists of 9 separate 70-Å regions in the yellow and red. All the exposures were 1 hour in duration.

The raw frames were reduced with Ritter Observatory’s standard reduction script under Sun/IRAF 2.11.3.² Removal of the telluric lines was done with the IRAF task *telluric*. The template spectra used in this context were artificial rows of Gaussians constructed from spectra of telluric standard stars taken under various conditions. For each spectrum of HD 199 478, the template that provided the best telluric correction was used. However, for a few spectra none of the templates in the library were completely successful at removing telluric lines. The spectra were then Doppler corrected to the heliocentric rest frame and normalised to the continuum.

2.2. Consistency check

An important point of any study which relies on observations collected at various observatories, with different instruments and equipment, is the mutual consistency among the corresponding datasets. The ideal way to perform a consistency

check is to compare strictly simultaneous data collected from different places.

Fortunately, our sample has three such spectra, that were taken at the NAO, TO and RO within 8 hours in the same night (Sept. 17, 2000). Using these spectra we checked for possible systematic differences in continuum and wavelength calibrations. The results obtained indicate that the wavelength calibration of the NAO and the TO spectra agree perfectly while the Ritter spectrum shows a one pixel systematic shift to the red.

On the other hand, and as regards photometric calibration, the Ritter spectrum (corrected for the shift of one pixel) fits quite well (within the noise) the NAO spectrum, while the relative fluxes between 6561 to 6584 Å in the TO spectrum are up to 3% stronger. Since the three spectra are not strictly simultaneous and since line profile variations on a shorter (hours) time scale cannot be excluded, it is not currently possible to judge to what extent the established differences in the fluxes redward of the emission peak of H α might be caused by imperfect continuum rectification or are due to real variability in the wind.

Thus, differences of $\sim 9 \text{ km s}^{-1}$ in velocity scale and up to 3% in relative flux cannot be excluded in our spectral time-series (but see next section).

3. Photospheric variability

3.1. Photometric evidence

Recent results (Percy et al. 2008) indicate that the photometric behaviour of HD 199 478 is characterised by continuous irregular/multi-periodic variations with an amplitude of about 0.15 mag on a time-scale of 20 to 50 days. In some observational runs colour variations of up to 0.05 mag, in phase with the light curve, have been also observed while in others no colour variations were detected above the corresponding error. In these properties HD 199 478 is similar to other OB SGs which are known to be photometrically variable and show small amplitude microvariations in the visual, with little colour variations, on a time scale from days to months (see e.g. Aerts et al. 1999; van Genderen 2001; Mathias et al. 2001).

3.2. Photospheric variability traced by C II doublet and He I 6678 lines.

Following Markova & Valchev (2000), we used the absorption lines of C II λ 6578.03, 6582.85, He I λ 6678.15 and He I λ 5875.67 to probe the deep-seated variability and photospheric structure of HD 199478 during the period covered

² IRAF is distributed by the National Optical Astronomy Observatories, which are operated by the Association of Universities for Research in Astronomy, Inc., under contract with the National Science Foundation.

by our observations. To improve the internal consistency of the wavelength scale in the extracted spectra from different observatories, which is of crucial importance for the purposes of the time-series analysis, the C II and He I $\lambda 6678$ line profiles were realigned using the diffuse interstellar band at $\lambda 6613.6$ as a fiducial. Similarly the interstellar line of Na I D $\lambda 5889.95$ was aligned for our study of profile changes in He I $\lambda 5876$. Following these adjustments, we estimate that the velocity scale local to each line profile is stable to 1–2 km s⁻¹. We are also confident that the C II lines are not severely affected by large fluctuations in the outer red wing of H α . For the photospheric analyses the C II lines were normalised to a local continuum assigned (using a low-order polynomial) between $\lambda 6570$ to 6590\AA .

Radial velocities of the selected He I and C II lines were measured by fitting Gaussian profiles in the knowledge that these lines are generally very symmetric. For the 2000 datasets the following estimates of the mean radial velocity and peak-to-peak amplitude were derived: -1.9 ± 3.9 km s⁻¹ and 16 km s⁻¹ for C II $\lambda 6578$; -2.0 ± 3.7 km s⁻¹ and 12 km s⁻¹ for He I $\lambda 6678$ and $+2.8 \pm 3.7$ km s⁻¹ and 13 km s⁻¹ for He I $\lambda 5876$. Variations of $\sim 15\%$ in the total equivalent widths of the lines were also established. There is a tighter correlation between the strength and velocity changes seen in C II and He I $\lambda 6678$ than between either of these lines and He I $\lambda 5876$.

The sampling rate of the 2000 (and the 1999) dataset is rather uneven and short-time series secured over a few days are separated by data gaps of between 1 to 3 months. This makes the search for periodic signals rather more uncertain. We applied the CLEAN method (Roberts et al. 1987) to the radial velocity measurements (using a gain of 0.5 and 200 iterations). The power spectra, where the features of the window function have been deconvolved using the discrete Fourier Transform, are shown in Fig 1, for the 1999 C II and the 2000 He I $\lambda 6678$ and C II data.

Clearly, there is no strictly periodic signal present in the photospheric lines of HD 199478 that remains coherent between 1999 to 2000. There is instead some indication that the absorption lines are semi-modulated in their central velocities over time-scales of \sim weeks to months. The only signal in the 2000 power spectrum that is consistent between C II and He I $\lambda 6678$ is at a frequency of ~ 0.085 days⁻¹, i.e. a period of ~ 11.7 days. Interestingly, in 1999 this modulation is essentially absent, but the strongest peak in the C II dataset at 0.0478 days⁻¹ corresponds to precisely twice the 11.7 days period. We find no evidence for a 11.7 days or 23.4 days modulation in He I $\lambda 5876$. However, note that the 1999 data sampling is more fragmented, with a gap of around 140 days. The central velocities of the C II and He I $\lambda 6678$ absorption lines phased on both these periods are shown in Fig 2.

Despite the high signal-to-noise and spectral resolution of our data (Sect. 2.2) there is also no evidence for sub-features travelling blue-to-red (prograde) in the absorption troughs of the lines, that might for example be identified in terms of the presence of low-order non-radial pulsations.

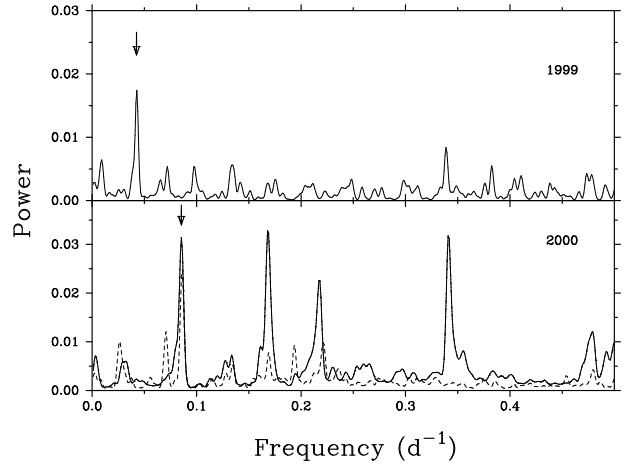


Fig. 1. Power spectrum (in arbitrary units) for the C II (solid line) and He I $\lambda 6678$ photospheric absorption lines. The arrow marks the ‘stable’ peaks at ~ 11.7 days and 23.4 days.

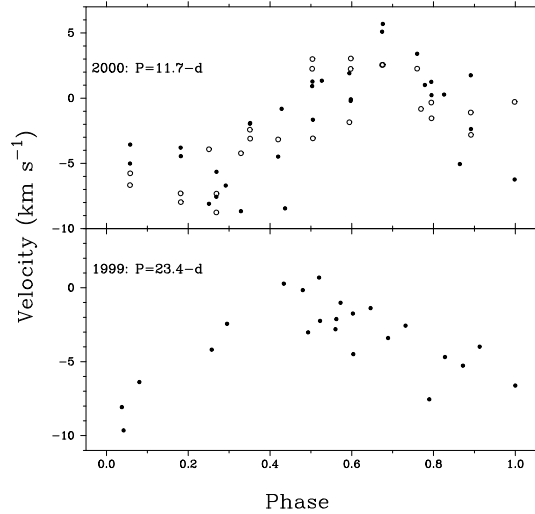


Fig. 2. The absorption central velocities of C II (filled circles) and He I $\lambda 6678$ (open circles) phased on the modulation time-scales identified in the 1999 and 2000 datasets.

3.3. Comparison between spectral and photometric variability

The 2000 differential *uvby* photometry obtained by SA as well as the 2000 *UBV* data collected by JP, though not strictly simultaneous, cover the same time period as the corresponding spectroscopic data. The Fourier and self-correlation analysis of these data indicate the presence of a periodic variation of 18 ± 4 (*UBV*) to 21 ± 4 (*uvby*) days with an amplitude of about 0.15 mag. The colour curve of this micro-variation is blue at the maxima and red at the minima of the light curve, thus resembling α Cyg variations in BA SGs.

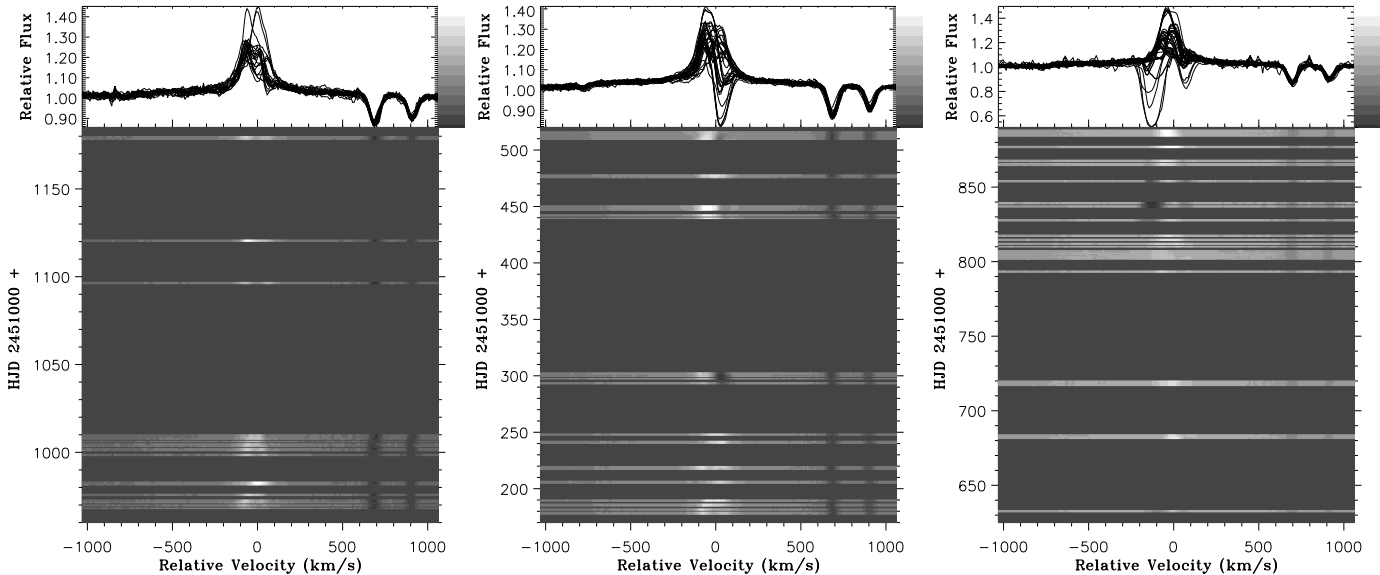


Fig. 3. —The 1998 (left), 1999 (middle) and 2000 (right) time-series of $H\alpha$ shown as one-dimensional plots (top) and two-dimensional grey scale images (bottom). All spectra have been corrected for $V_{\text{sys}} = -12 \text{ km s}^{-1}$. Velocity scale given with respect to the rest wavelength of $H\alpha$.

The estimated photometric period is somewhat larger but still consistent (within 3σ) with the 11.7 day period variation in radial velocity of C II and He I $\lambda 6678$ photospheric lines. This finding strongly suggests that the same physical mechanism (based in the stellar photosphere) is most likely responsible for the two phenomena observed, which might be identified as the signatures of pulsations.

However, note that the interpretation of the photospheric variability of HD 199478 reported here and in Percy et al. (2008) is not straightforward in terms of pulsation. On the one hand, radial pulsations are not likely since: first, the period is not stable between the observing runs carried out in different years and second, with only one exception, the estimated periods are longer than the radial fundamental pulsational period, $P_{\text{rad, fund}} \sim 8$ days, as derived by Markova & Valchev (2000). On the other hand, the irregular character of this variability is quite similar to that observed in other late B SGs and A-type stars (Kaufer et al. 1997). A possible origin for these variations, at least for stars with $M_{\star} \leq 40 M_{\odot}$, is the action of non-radial oscillation modes excited by the opacity mechanism.

In this respect, we note that:

- i) a period of about 20 days, as derived from photometric and spectroscopic data of HD 199478, is fully consistent with the value inferred via the period-luminosity relation for B-type variables with excited g -mode oscillations (Fig. 2 in Waelkens et al. 1998);
- ii) on the HR diagram with parameters derived with FASTWIND, HD 199478 elegantly joins the group of B-type SGs studied by Burki (1978) for which g -mode instability is suggested to explain their variability (Fig. 3 of Waelkens et al. 1998).

Therefore, non-radial g -mode oscillations might explain the photospheric variability of HD 199478. But our data lacks evidence for travelling blue-to-red (prograde) features within the absorption troughs of the lines, which normally indicate non-radial pulsational behaviour.

Clearly, very extended time-series datasets are requisite for extracting reliable long period signals from the irregular absorption line changes which characterise B SGs. These targets lend themselves particularly to modest-sized robotic telescopes equipped with high-resolution spectrographs.

4. Wind variability

4.1. $H\alpha$ monitoring campaigns in 1999 and 2000

In Figure 3 the $H\alpha$ time-series for 1999 and 2000 are shown as two-dimensional gray-scale images. Above each of the velocity-time frames the corresponding one-dimensional spectra are plotted to provide a visual assessment of the size of the fluctuations at each velocity bin. Gaps between observations, if equal or larger than 1.0 day, are represented by black bands. All spectra have been corrected for the systemic velocity, $V_{\text{sys}} = -12 \text{ km s}^{-1}$. The zero point in velocity corresponds to the rest wavelength of $H\alpha$. A similar plot, illustrating the $H\alpha$ time-series obtained in 1998 (from Markova & Valchev 2000), is also provided for completeness.

Figure 3 demonstrates that the $H\alpha$ profile of HD 199478 is strongly variable, exhibiting a large diversity of profile shapes and behaviour patterns. In particular, and as also noted by Markova & Valchev (2000), in June-July, 1998 as well as during the first two months of 1999, the profile appeared fully in emission evolving from a double-peak morphology with a blue component that is stronger than the red one, to a single-peaked feature centered almost at the rest frame. Some hints

about the subsequent development of this feature to the red seem also to be present. Three such cycles have been identified by Markova & Valchev (2000) (see left and middle panels of Figure 3): the first - between HJD 2450968-982; the second - between HJD 2450998-1009 and the third - between HJD 2451178-189. Another cycle taking place between HJD 2451217-247 can now be easily recognised thanks to the new observations in March 1999. This finding implies that the variability pattern described above is relatively stable (over at least 9 months) with a characteristic time-scale of about 15 days and a possible re-appearance after one month or longer.

A new variability pattern is revealed by the 1999 and 2000 observations, where $H\alpha$ appears not only in emission, but also in partial or complete absorption. In particular, on HJD 2451293 (April 24, 1999) in addition to the blue-shifted emission ($V_r = -75 \text{ km s}^{-1}$) a slightly red-shifted absorption feature ($V_r = +40 \text{ km s}^{-1}$) has appeared giving rise to a reverse P Cygni profile. The latter persisted for at least 8 days, growing slightly stronger in intensity.

About five months later, namely on HJD 2451439 (Sept. 17), $H\alpha$ is seen fully in emission again, though with a weak dip at about $+60 \text{ km s}^{-1}$, which makes the profile appear double-peaked with a blue component being much stronger than the red one. This configuration was preserved for at least 7 days, i.e. up to HJD 2451449. On HJD 2451475 the absorption dip is missing but one month later it appears again, stronger than before, and persists for at least 6 days (between HJD 2451509-515) during which time the profile again looks like a reverse P Cygni. Interestingly, the second appearance of the dip is exactly at the same position as the first one suggesting the same physical origin for both events.

The 2000 observations importantly revealed (right panel of Figure 3) the presence of another unusual event during which $H\alpha$ changes suddenly and drastically from pure emission to pure absorption and back to pure emission. By chance, the distribution of the available observations in time was quite good allowing the development of this spectacular event to be followed in more detail.

In Figure 4 one can see that before the onset of the high-velocity absorption (HVA) event, $H\alpha$ appeared fully in emission developing from a double-peaked to a single-peaked morphology and strengthening slightly with time (HJD 2451792-816). On HJD 2451827, in addition to the emission a localised high-velocity ($V_r = -150 \text{ km s}^{-1}$) absorption extending from -68 to -250 km s^{-1} is present making the profile appear P Cygni-like. Over the next 9 days the P Cygni feature evolves into double absorption with central emission where the blue component is significantly stronger and wider than the red one. Two weeks later, (HJD 2451863) the morphology of the profile is still the same though the blue component is weaker and narrower while the red one has apparently strengthened becoming somewhat wider. Subsequently the two absorptions are fading in parallel and disappear completely on HJD 2451877. Our observations further suggest that the absorption event seen in the $H\alpha$ time-series of HD 199478 between HJD 2451827 – 876 may not be unique. Indeed, readers should note that on HJD 2451632 (see right panel of Figure 3) $H\alpha$ has also appeared as a double absorption feature. Unfortunately, due to poor temporal coverage

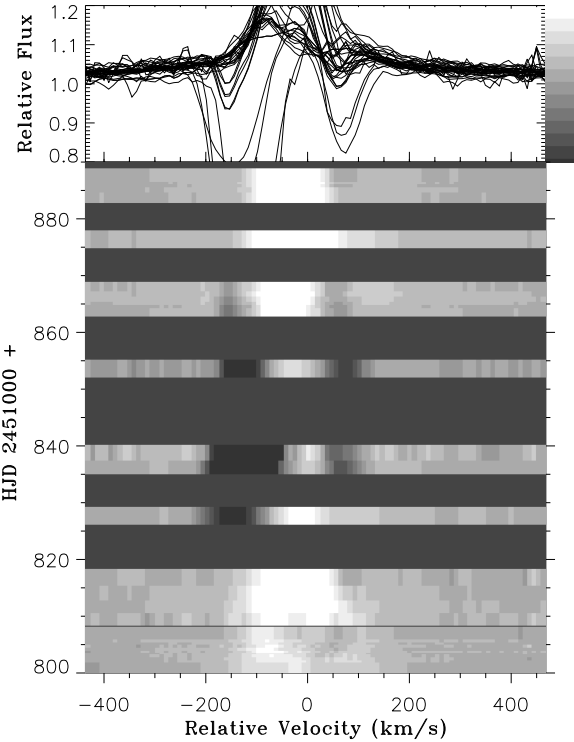


Fig. 4. HVA event observed in the $H\alpha$ data of HD 199478 in 2000.

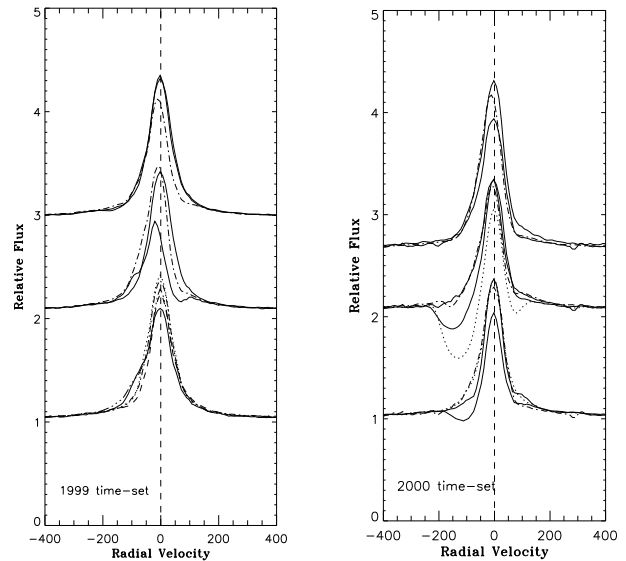


Fig. 5. Top: $H\alpha$ profile of HD 199478 illustrating the behaviour of pure wind contribution to the line (in velocity space).

the time development of this feature cannot be followed, but given the similarity in the morphology of this profile and the one taken, e.g., on HJD 2451853 we are tempted to speculate that about 6 months earlier an absorption phenomena similar to the one recorded in September - October 2000 may have occurred in this star.

4.2. Wind contribution

To probe further the nature and origin of peculiar emission and HVAs in the $H\alpha$ data of HD 199478 we normalised the observed $H\alpha$ profiles to a constant photospheric profile³ computed by means of the FASTWIND code with parameters from Markova & Puls (2008) (given also in Table 4).

In Figure 5 the $H\alpha$ profiles from the 1999 and 2000 datasets are shown (in chronological order from the bottom upwards). Profiles from runs separated by large gaps are grouped together where periods without significant lpv are represented by a single averaged profile so as not to confuse the figure.

The following points are immediately apparent from these plots:

- Outside the HVA events the wind contribution can be assigned to two components: (i) a strong emission feature which is either symmetric with respect to the stellar rest frame or shows weak blue-to-red asymmetry with a blue wing being more extended and stronger than the red one and (ii) localised emission bumps with variable position which more likely give rise to the established V/R variations.
- During the HVA episodes (right panel, bottom and middle groups) in addition to the extended blue-shifted absorption an emission component also exists, i.e. the wind does not only absorb but also emits $H\alpha$ photons, contrary to the cases described by Kaufer et al. (1996b), where the HVAs are not accompanied by unshifted emission.
- The red-shifted absorption seen occasionally in $H\alpha$, is more likely of wind origin and suggests the presence of matter infall at the base of the wind.

From the properties outlined above one might conclude that the envelope of HD 199478 consists of (i) a spherical component where the physical conditions favour only processes which produce emission in $H\alpha$ and (ii) localised large-scale wind structures with matter infall and outflows, where emission and/or absorption can originate.

4.3. Comparisons of high-velocity absorption event in HD 199478 to those in other late-B SGs

Comparison of our Figure 4 with similar results from Kaufer et al. (1996a,b) showed that the spectacular absorption event seen in $H\alpha$ of HD 199478 is qualitatively similar to the HVAs observed in HD 34085 (B8 Ia, β Ori), HD 91619 (B7 Ia) and HD 96919 (B9 Ia), though with one exception: in our data-set the blue and the red-shifted absorption components do not merge to form an extended blue-to-red absorption, as is the case of the objects Kaufer et al. studied, but instead occur parallel to each other (though we accept the caveat that a more intensive and extended dataset is ideally required).

That the spectacular phenomena of HVAs in $H\alpha$ have been observed so far in 4 late B SGs with peculiar emission in $H\alpha$ deserves special attention since it might indicate some fundamental property of their stellar winds. With this in mind we followed Kaufer et al. (1996b) and measured the main properties

³ Such an approximation is legitimate since the observed photospheric variability in HD 199478 is indeed very weak (see Sec. 3.2)

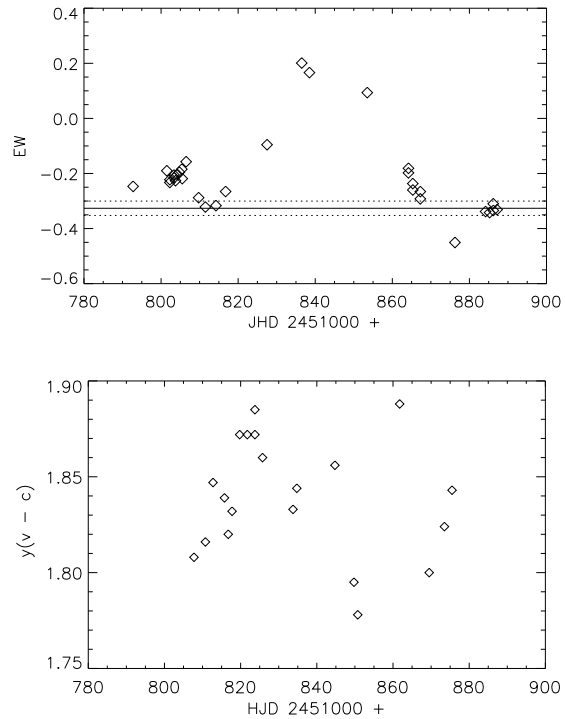


Fig. 6. Top: Total equivalent width of the $H\alpha$ line profile of HD 199478 during the 2000 HVA event as a function of time. The horizontal lines represent the "undisturbed" mean equivalent width of $H\alpha$ (fully-drawn) and its corresponding standard deviation (dotted). Bottom: Time behaviour of the differential y -magnitudes during the HVA event

Table 3. Properties of HVAs in $H\alpha$ observed in 3 late-B SGs. Data for HD 34085 and HD 96919 are taken from Kaufer et al. (1996b). All velocities, measured with respect to the stellar rest frame, are given in units of the corresponding wind terminal velocities (from Table 4).

	HD 34085	HD 96919	HD 199478
Signature	1994	1995	2000
MJD of max. blue depth	2449493	2449792	2451836
Max depth in % of cont	20	70	49
Vel. of max. depth	0.40...0.60	0.29...0.43	0.37...0.76
Blue-edge velocity	0.79...1.20	0.43...0.64	0.68...1.39
Red-edge velocity	0.34...0.52	0.32...0.48	0.41...0.84
Rise time of W_λ [d]	11	21	22
Decay time of W_λ [d]	20	46	33
Duration of event [d]	40	90	55

(such as, e.g., relative intensity, position and blue- and red-edge velocities) of the 2000 HVA in $H\alpha$ of HD 199478 at the time of its maximum intensity. Based on the time evolution of the $H\alpha$ total equivalent width (measured by integrating the flux between 6554 and 6570 Å) we determined the total duration and the rise and decay times of this event (Figure 6, top panel)

The estimates thus derived are listed in Table 3 together with similar data for HD 34085 and HD 96919 (from

Kaufer et al. 1996b). Note that since in our spectra the blue-shifted component of the HVA event never merges with the red-shifted one, the red-edge velocity (given in Table 3 in bold) does not refer to the extended blue-to-red absorption (as is the case of Kaufer et al. 1996b) but instead corresponds to the red-absorption component itself. Note also that due to the large uncertainties in the adopted terminal velocities (see next section) the normalised velocities sometimes exceed unity.

Compared to similar events in HD 34085 and HD 96919, the HVA seen in HD 199478 is of intermediate duration and strength. Its time development is roughly consistent with results from Kaufer et al., which show rise times that are smaller than the decay times.⁴ Thus, the duration of a HVA event seems to depend on its maximum strength (stronger maximum absorption – longer duration), while its development in time (rising time vs time of decay) appears to be independent of this parameter. In addition, the blue-edge velocity and the velocity of maximum depth of a HVA event may anti-correlate with its strength, i.e. stronger features tend to reach maximum depth at lower velocities, being less extended in velocity space than weaker ones. Furthermore, and as also noted by Israelian et al. (1997), the maximum positive velocity of a HVA is always lower than the corresponding maximum negative velocity. (Due to the limited number of stars these results can only be regarded as suggestive and they have to be confirmed with improved statistics.)

Finally, we note that the photometric behaviour of HD 199478 during the 2000 HVA event in $H\alpha$ provides tentative evidence that at the onset of the event the star was about one magnitude fainter than at the moment of maximum line absorption (Figure 6, bottom panel).

5. Stellar and wind parameters of late-B stars which have exhibited HVAs in $H\alpha$

To help understand the nature and origin of the $H\alpha$ variability, especially the appearance of HVAs, Kaufer et al. (1996a) have determined the fundamental parameters of their sample stars employing:

- i) the Azzopardi spectral type–absolute magnitude and observed $H\gamma$ equivalent width–absolute magnitude calibrations (Azzopardi 1981);
- ii) the Schmidt-Kaler spectral type–bolometric correction and spectral type –effective temperature calibrations (Schmidt-Kaler 1982);
- iii) the evolutionary tracks of Schaller et al. (1992) to derive stellar masses;
- iv) the maximum half-width of the TVS of two isolated absorption lines to estimate projected rotational velocities; see also (Reid et al. 1993)
- v) the UV resonance lines Mg II $\lambda\lambda 2795, 2803$ to determine wind terminal velocities, v_∞ .

By means of these parameters the authors have subsequently constrained the true rotational periods (by means of

$P_{\text{rot}}/\sin i$ and $P_{\text{rot,break}}$) and evaluated the radial fundamental pulsational periods of the stars. The analysis led the authors to suggest that rotation plays an important role in determining the properties of the $H\alpha$ variability including the HVA events.

Prior to the use of currently available state-of-art model atmosphere codes, the approach used by Kaufer et al. (1996a) (with its well-known weaknesses and uncertainties) was the only one to permit the basic parameters of hot stars to be determined.

The situation has changed drastically since then and stellar and wind parameters of hot stars can now be derived with relatively high precision using the methods of the quantitative spectral analysis. The outcomes of such analyses, performed by means of the present day NLTE, line blanketed model atmosphere codes (e.g. CMFGEN Hillier & Miller 1998 and FASTWIND Puls et al. 2005) have unambiguously showed that the newly derived stellar and wind parameters can significantly deviate from their earlier determinations (e.g., Martins et al. 2005 and references therein for O stars and Crowther et al. 2006; Markova & Puls 2008; Searle et al. 2008 for B stars)

With this in mind and given the limited number of late B SGs with reliably determined stellar and wind parameters (see Markova & Puls 2008 and references therein), we decided to re-determine the parameters of the Kaufer et al. late-B SGs with HVAs in $H\alpha$, using optical spectra kindly provided by Otmar Stahl and employing the one of the latest version of the FASTWIND code. This way a homogeneous data base for late B SGs sharing similar empirical properties in $H\alpha$ would be created, which might be easily extended in the future.

To perform our analysis we followed the strategy outlined in detail by Markova & Puls (2008). In particular, effective temperatures, T_{eff} , were estimated from the Silicon ionization balance, fitting the Si II doublet at 4130 Å and the Si III triplet at 4552 Å and adopting a solar Silicon abundance ($\log(\text{Si}/\text{H}) = -4.45$ by number⁵, cf. Grevesse & Sauval 1998 (and references therein), and a microturbulent velocity, v_{mic} , appropriate for the corresponding spectral type (Markova & Puls 2008). Since in all objects the blue wing of $H\gamma$ seems to be affected by blue-shifted wind emission (similar to the one seen in $H\alpha$) surface gravities, $\log g$, were derived fitting the wings of $H\delta$. The accuracy of these estimates is ± 500 K in T_{eff} and ± 0.1 in $\log g$.

Projected rotational and macroturbulent velocities, $v \sin i$ and v_{mac} , – these parameters were determined from Mg II $\lambda 4481$ employing the Fourier technique developed by Simon-Diaz & Herrero (2007). Since this method provides only rough estimates of v_{mac} the latter have been additionally adjusted during the fitting procedure (if necessary) to improve the quality of the fits. Radial velocities from Kaufer et al. (1996a) have been adopted.

⁴ This result has to be considered with caution since the exact time of maximum depth absorption in HD 199478 is not known with confidence due to limited time-series coverage.

⁵ According to latest results (Asplund et al. 2005), the actual solar value is slightly lower, $\log(\text{Si}/\text{H}) = -4.49$, but such a small difference has no effect on the quality of the line-profile fits.

Table 4. Stellar and wind parameters of HD 34 085 (β Ori) and HD 96 919 as derived in the present study employing the FASTWIND code. Numbers in brackets refer to similar data from Kaufer et al. (1996a). Estimates for HD 199 478 are taken from Markova & Puls (2008). Effective temperatures are given in kK, velocities in km s⁻¹, time periods in days. Estimates for \dot{M} and $\log D_{\text{mom}}$ are lower limits.

star	sp	distance	M_V	T_{eff}	$\log g$	R_*/R_\odot	$\log L/L_\odot$	M_*/M_\odot	$\log \dot{M}$	$\log D_{\text{mom}}$
HD 91 619	B7Iae	2.51	-7.00(-7.99)	13.9(12.2)	1.85(1.75)	63(114)	5.13(5.42)	11(27)	-6.92±0.32	27.18±0.33
HD 199 478	B8Iae	1.84	-7.00	13.0	1.70	68	5.08	9	-6.73...-6.18	27.33...27.88
HD 34 085	B8Iae	0.50	-8.31(-7.77)	12.5(11.2)	1.70(1.67)	129(116)	5.56(5.28)	31(23)	-6.47 ^{+0.27} _{-0.15}	27.75 ^{+0.27} _{-0.20}
		0.24 ^a	-6.70			61	4.92	7	-6.96 ^{+0.37} _{-0.30}	27.10 ^{+0.37} _{-0.32}
HD 96 919	B9Iae		-7.0*(-7.97)	11.0(10.3)	1.50(1.50)	71(141)	4.82(5.30)	6(23)	-7.10 ^{+0.25} _{-0.13}	27.03 ^{+0.27} _{-0.21}
star	V_{sys}	v_{mac}	v_{mic}	$v \sin i$	V_{break}	$P_{\text{rot}, \text{break}}$	$P_{\text{rot}}/sini$	v_{esc}	v_∞	
HD 91 619	-6	35	8	35(60)	153(212)	21(27)	91(96)	220(261)	170...330	
HD 199 478	-12	40	8	41	134	25	84	191	170...350	
HD 34 085	+18	35	8	30(55)	184(195)	35(30)	218(107)	262(244)	230...350	
					129	24	103	183	230...350	
HD 96 919	-24	25	7	30(60)	112(176)	32(40)	120(119)	160(220)	250...370	

^a - *HIPPARCOS* distance estimate

* - absolute magnitude from the calibration of Humphreys & McElroy (1984)

Stellar radii, R_* – These parameters were determined from the derived effective temperatures and de-reddened absolute magnitudes (see, e.g., Kudritzki 1980). The latter were calculated using standard extinction law with $R = 3.1$ combined with: (i) visual magnitudes, V , and $B - V$ colours from the *HIPPARCOS Main Catalogue (I/239/hipmain)*; (ii) intrinsic colours $(B - V)_0 = -0.03$ from (Fitzpatrick & Garmany 1990), and (iii) distances collected from various sources in the literature.

In particular, for HD 91 619, a member of Car OB1 association, a distance of 2.51 kpc as provided by Humphreys (1978) was adopted. For HD 34 085 (β Ori) the situation is a bit more complicated. As a member of Ori OB1 this star should be situated at about 0.5 kpc (Humphreys 1978). Its possible membership of the τ Ori R1 complex (Hoffleit & Jaschek 1982) reduces the distance to about 0.36 kpc, while the *HIPPARCOS* distance estimate is 0.24 kpc. ⁶ Thus, for β Ori we provide two entries as upper and lower limits to the distance to account for all possibilities. For HD 96 919, which does not belong to any cluster or association, an absolute magnitude according to the calibration of Humphreys & McElroy (1984) was adopted. We quote typical uncertainties of ± 500 K in our T_{eff} estimates and of ± 0.4 in M_V (for members of associations) to 0.5 mag (for stars with M_V from calibration) (Markova & Puls 2008). The error in the stellar radius is dominated by uncertainties in M_V and is of the order of $\Delta \log R_* = \pm 0.08...0.10$, i.e., less than 26% in R_* .

Luminosities, $\log L/L_\odot$, and stellar masses, M_* , – these values were determined from the corresponding T_{eff} and R_* values and the “true” surface gravities, respectively. ⁷ The

⁶ Below 0.5 kpc the *HIPPARCOS* distance estimates are generally accepted as reliable.

⁷ “True” gravity results from the observed gravity corrected for the centrifugal acceleration ($= (v \sin i)^2 / R_*$). Due to the lower $v \sin i$ of

typical uncertainties of these estimates are $\Delta \log L/L_\odot = \pm 0.17$ to 0.22 and $\Delta \log M_* = \pm 0.19$ to 0.22.

Terminal wind velocities, v_∞ , – values for β Ori and HD 96 919 have been determined from the blue-edge of the Mg II resonance lines at $\lambda\lambda$ 2795, 2803 by Kaufer et al. (1996a). However, the authors note that due to the absence of sharp blue edges, their estimates have to be considered as lower limits only. Thus, in these two cases we adopted the Kaufer et al. estimates of v_∞ (i.e. ~ 230 km s⁻¹ for HD 34 085 and ~ 250 km s⁻¹ for HD 96 919) but assumed an asymmetric error of +50% to allow for a rather large uncertainty towards higher values. For HD 91 619, since no v_∞ estimate was found in the literature, we followed Markova & Puls (2008) and adopted $v_\infty = v_{\text{esc}} = 220$ km s⁻¹ assuming an asymmetric error of -25/+50%.

Mass-loss rates, \dot{M} , and velocity exponent β – In the case of strong *undisturbed* winds ($H\alpha$ in emission) \dot{M} and β can be estimated, with relatively high precision, from the best fit to the red wing and the peak emission of the $H\alpha$ profile, respectively. Indeed, $H\alpha$ is in emission in the spectra of HD 91 619 and HD 96 919 available to us. However, and as also shown in Figure 7, such profiles cannot be reproduced in terms of spherically symmetric smooth wind models since at this temperature regime the models predict profiles in absorption partly filled in by wind emission. Due to this reason only lower limits to \dot{M} are derived for our sample stars, with β ranging from 0.8 to 1.5, except for HD 96 919 where an upper limit to β of 1.3 was adopted (see Markova & Puls 2008). Under these circumstances any excess emission seen in $H\alpha$ should be attributed either to deviations from spherically symmetric wind approximations and/or to processes different from recombination (see sect. 6).

the sample stars this correction is generally small, between 0.01 to 0.03.

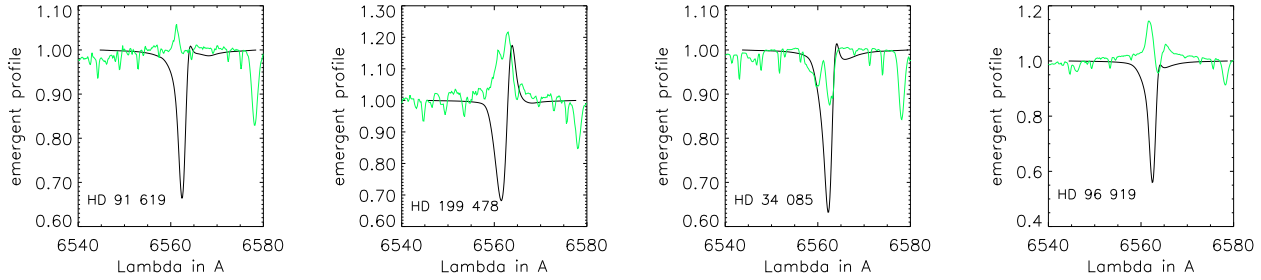


Fig. 7. Examples of typical $H\alpha$ profiles observed in the four sample stars which have been recognised to show HVA events. Over-plotted are synthetic profiles accounting for the contribution of photospheric absorption plus spherically symmetric smooth wind emission (for more info see text.)

The errors in our \dot{M} estimates (actually in $\log Q$) accumulated from uncertainties in β and in R_\star are typically less than 0.30 dex. Having R_\star , \dot{M} and v_∞ thus determined we finally calculated the modified wind momentum, $D_{\text{mom}} = Q v_\infty R_\star^2$, with a typical error $\Delta \log D_{\text{mom}}$ between 0.13...0.35 dex.

5.1. Comparisons to parameters derived in other investigations.

Stellar properties derived in our analysis, together with the data for HD 199 478 (from Markova & Puls 2008), are listed in Table 4. Estimates from Kaufer et al. (1996a) are also provided (numbers in brackets) for comparison.

Compared to similar data from Kaufer et al.:

- Our $v \sin i$ estimates are about a factor of 0.5 lower. This result is easy to interpret since our estimates account for the effects of macroturbulence. Contrary to what might be expected, the lower values of $v \sin i$ did not result in significantly different values of the rotational period (see Table 4). With our approach the decrease in $v \sin i$ is almost completely compensated by an increase in R_\star (see below).
- Our T_{eff} and $\log g$ estimates are surprisingly similar to those in Kaufer et al. This finding indicates that in these particular cases the effects of line blanketing are not too large (as also shown by Markova & Puls 2008) and that in the Kaufer et al. approach the effects of the larger stellar masses have been to a large extent compensated by the larger radii.
- Our R_\star and $\log L/L_\odot$ are significantly lower than those of Kaufer et al. The reason for this is the large difference in the adopted absolute magnitudes: according to our estimates the three stars are about one magnitude fainter than estimated via the Azzopardi calibrations (apart from HD 34 085 (β Ori), first entry, where there is an alternative possibility of M_V being half a magnitude brighter). Such large differences in M_V cannot be solely explained by differences in the methods used, but might indicate instead problems with the Azzopardi calibration (see also Markova & Puls 2008).
- In general, our estimates of M_\star tend to be lower (by about 0.39 to 0.58 dex) than those estimated by Kaufer et al. via the evolutionary tracks (apart from the first entry for β Ori, where a value of 0.12 dex larger was derived). This finding is consistent with similar results from previous investigations

(Crowther et al. 2006; Trundle et al. 2005; Markova & Puls 2008) which also indicate a mild “mass discrepancy” for B SGs. Indeed, the differences established here are somewhat larger, but in their study Kaufer et al. used evolutionary tracks which do not take into account the effects of stellar rotation, e.g., Schaller et al. (1992), while in all other studies evolutionary tracks from Meynet & Maeder (2000) (with stellar rotation) have been used instead.

On the other hand, the stellar radii and luminosities derived in the present study are consistent with similar results from Markova & Puls (2008). In particular, they fit very well (within the existing scatter) the $\log T_{\text{eff}}-R_\star$ and $\log T_{\text{eff}}-\log L/L_\odot$ distributions derived by these authors for Galactic B SGs. The only real outlier is HD 34 085 (β Ori), first entry, where larger deviations (~ 0.6 dex in $\log L/L_\odot$ and a factor of 2 in R_\star) have been established. Since the $\log g$ -value of this star is typical for a late SGs we suggest that the photometric distance provided by Humphreys (1978) is overestimated.

Finally, strong agreement (within the corresponding errors) was found between our T_{eff} , $\log g$ and v_{mic} estimates of HD 34 085 (β Ori) and those derived by Przybilla et al. (2006) via a hybrid non-LTE technique ($T_{\text{eff}} = 12\,000 \pm 200$ K, $\log g = 1.7 \pm 0.1$, $v_{\text{mic}} = 7 \pm 1$ km s $^{-1}$) Good agreement was also found with the results from Israelian et al. (1997) for HD 34 085 ($T_{\text{eff}} = 13\,000$, $\log g = 1.6$ and $v_{\text{mic}} = 7$) obtained via the NLTE unblanketed plane-parallel hydrostatic code TLUSTY (Hubeny 1988). The latter indicate that at these temperatures the effects of line blocking/blanketing are small as also found by Markova & Puls (2008) and that in the particular case of this star the wind effects also seem to be minimal⁸.

6. Discussion and conclusions

Extensive monitoring campaigns of several late-B SGs, namely HD 199 478 (present study as well as Markova & Valchev 2000) and HD 91 619, HD 34 085 and HD 96 919 (Kaufer et al. 1996a,b, 1997; Israelian et al. 1997), indicate that their $H\alpha$ profiles exhibit quite similar peculiarities, consisting of a double-peaked emission with V/R variation and occasional episodes of strong absorption indicating simultaneous mass infall and out-

⁸ (Although the somewhat lower value of $\log g$ of Israelian et al. more likely results from the neglect of the wind effects)

flows. Such line signatures cannot be reproduced by conventional (i.e. non-rotating, spherically symmetric, smooth) wind models, which instead predict profiles in absorption partly filled in by emission for SGs at this temperature regime.

Discrepancies between observed and predicted $H\alpha$ profiles have been also established for many O and *early* B SGs, where this finding was usually interpreted as an indication for deviations from the adopted spherically symmetric, smooth wind approximations (e.g., Morel et al. 2004; Markova et al. 2004, 2005 and references therein).

Following this reasoning, axially symmetric envelopes, modulated, at least in the inner parts, by co-rotating weak magnetic structures have been assumed to explain the appearance and kinematical properties (e.g. double-peaked morphology with V/R variations) of the peculiar $H\alpha$ emission in the spectra of the four late-B SGs noted above (Kaufer et al. 1996a; Markova & Valchev 2000).

In addition, to account for the sudden appearance of HVAs in $H\alpha$ and their development in time (e.g. the fast rise over a large velocity range, the lack of unshifted line emission, and the mooted re-appearance over a rotational time-scale), episodic and azimuthally extended, density enhancements in the form of co-rotating spirals rooted in the photosphere (Kaufer et al. 1996b) or closed magnetic loops similar to those in our Sun (Israelian et al. 1997) were also suggested.

It is generally mooted that non-radial pulsations (NRPs) and surface magnetic spots may equally be responsible for creating large-scale inhomogeneities in hot star winds (Fullerton et al. 1996). However, despite some progress (e.g., Kaufer et al. 2006) no convincing evidence of a direct relation between the time-scale of a given cyclical (wind) lpv and the predicted time-scale of recurrent surface features due to a specific pulsation mode, has been derived to date (see Townsend 2007 and references therein).

Note in the particular case of the four stars discussed here, non-radial pulsations due to g -modes oscillations were suggested to explain absorption lpv in their spectra (Kaufer et al. 1997; Markova & Puls 2008). This possibility is partially supported by the present results, which indicate that on the HR diagram, and for parameters derived with FASTWIND, these stars fall exactly in the region occupied by known variable B SGs, for which g -modes instability was suggested. Also, the photometric variability of HD 199 478 seems to be consistent with a possible origin in terms of g -mode oscillations (Percy et al. 2008). Thus, it seems very likely that the four late-B SGs in our sample are non-radial pulsators. Although no clear evidence of any causality between photospheric and wind (as traced by $H\alpha$) variability has been seen so far for these objects (present study as well as Kaufer et al. 1997), one might speculate that their winds are perturbed due to pulsational instability, with specific signatures seen in the behaviour of $H\alpha$.

An alternate possibility is that magnetic fields could be responsible for the appearance of large-scale structures and wind asymmetries in hot stars. In particular, magneto-hydrodynamical (MHD) simulations for stars with moderately strong rotation, and for stellar and wind parameters typical for O and early B SGs (plus a magnetic dipole aligned to the stellar rotation) showed that depending on the magnetic

Table 5. Magnetic field strength, B (in G), required to get an equatorial confinement with simultaneous mass infall and outflows around each of our targets. The Keplerian, R_K , the Alfvén, R_A , and the escape, R_E , radii (in units of R_\star above the photosphere) are calculated following Owocki & ud-Doula (2003). The HD 34 085 estimates correspond to the 2nd entry in Table 4.

Parameters	91 619	199 478	34 085	96 919
R_K	0.37	0.45	0.38	0.42
R_A	0.83..3.73	0.77..4.59	0.83..3.79	1.0..4.13
R_E	3.77	4.58	3.81	4.18
B ($R_K < R_A < R_E$)	5..100	5..180	5..105	5..85

spin-up, an equatorial compression, dominated by radial *infall* and/or *outflows* can be created, with no apparent tendency to form a steady, Keplerian disk (Owocki & ud-Doula 2003; ud-Doula, Owocki & Townsend 2008).

Indeed, due to the lack of strong convection zones associated with hydrogen recombination, normal (i.e. without any chemical peculiarities) hot stars are generally not thought to be magnetically active. However, theoretical considerations (e.g. Cassinelli & Macgregor 2000) supported by more recent observations (Bychkov, Bychkova and Madej 2003; Hubrig et al. 2007) indicate that this may not necessarily be true and that relatively strong, stable, large-scale dipole magnetic fields are present in different groups of B stars (e.g. SPB, Be, β Cep itself etc.)

Thus, it seems likely that in at least some hot stars magnetic fields can be an alternative source of wind perturbations and asymmetries. The potential role of magnetic fields in B SGs remains intriguing, especially because it might provide a clue to understand the puzzling problem of the simultaneous presence of red- and blue-shifted absorption in $H\alpha$ profiles of the four late-B SGs discussed here.

Guided by these perspectives, we employed the scaling relations given in Owocki & ud-Doula (2003) and calculated the Alfvén, R_A , the Keplerian, R_K , and the “escape”, R_E , radii of our targets, using data from Table 4 and fixing the magnetic field strength at the values required to create an equatorial confinement. Interestingly, the results listed in Table 5, show that in all four cases a very weak dipole magnetic field can effectively channel the wind outflows, leading to the formation of an equatorial compression with simultaneous radial mass infall and outflow.

With this in mind, new MHD simulations for the case of mid/late-B SGs have been recently initiated. The preliminary results (private communication, Asif ud-Doula) indicate that a pure dipole magnetic field of only a few tens of Gauss is indeed required to obtain a *cool* equatorial compression (with mass infall and outflow) around a rotating star with stellar and wind parameters as derived with FASTWIND for HD 199 478. (More detailed information about the outcomes of this study will be provided in a forthcoming paper.)

An obvious advantage of the model described above is that it has the potential to at least qualitatively account for some of

the puzzling properties of the $H\alpha$ line of our targets. In particular, the sudden appearance of red and blue-shifted absorptions might be explained if one assumes, that due to some reason the plasma in the infalling or outflowing zones of the compression or in both of them (during the HVA episodes) can become optically thick in the *Lyman* continuum and $L\alpha$, thus forcing $H\alpha$ to behave as a resonance line, i.e. to absorb and emit line photons. The kinematic properties of the resulting absorption features⁹ are difficult to predict from simple qualitative considerations but it is clear that these properties cannot be dominated by stellar rotation, but instead will be controlled by the physical conditions inside the compression.

Concerning the interpretation of the peculiar $H\alpha$ emission, the situation is more complicated since such emission can originate from different parts of the envelope under quite different physical conditions. For example, one can expect that the cool, less dense plasma outside the compression will only emit line photons (via recombinations), producing pure emission feature(s) in $H\alpha$.

Also, the cool equatorial compression might contribute to the $H\alpha$ emission, providing the plasma inside the compression can occasionally become optically thin in this line. However, note that even a plasma that is optically thick in $L\alpha$ and *Lyman* continuum can, under specific conditions, produce *pure* emission profiles in $H\alpha$ (e.g. *if* collisions dominate the $H\alpha$ formation or *if* due to some reasons the 2nd and 3rd levels of Hydrogen go into LTE (Petrenz and Puls 1996)).

Therefore, very weak dipole magnetic fields might be responsible for creating wind structures in the envelopes of late-B SGs. The models derived via MHD simulations seem to have the potential to account, at least qualitatively, for some of the peculiar characteristics of $H\alpha$ in the spectra of our targets. However, more detailed quantitative analysis is required to investigate this possibility further.

New high signal-to-noise observations to prove/disprove the presence of weak magnetic fields can help to clarify the picture. Of course, due to the low strength of the magnetic fields required one cannot expect to detect these fields directly but indirect evidence such as e.g., the detection of X-ray emission, abundance anomalies, specific periodic variations in UV resonance lines, interferometric observations (for more information see Henrichs 2001), might also be considered. Note that a weak longitudinal magnetic field of about $130 \pm 20 G^{10}$, might have been detected in HD 34 085 (β Ori) (Severny 1970), but confirmation is lacking.

Finally, at the cooler edge of the B-star temperature regime pure emission profiles in $H\alpha$ can be accounted for if one assumes the winds are clumped. Indeed, a spherically symmetric, clumped wind will mimic wind densities higher than the actual ones, thus giving rise to strong line emission, similar to that in O stars. Such winds may also give rise to wind absorption, providing some of the clumps are optically thick in $H\alpha$.

Detailed numerical simulations and line formation calculations are required to discriminate between the different possibilities.

Acknowledgements. This work was partly supported by the National Scientific Foundation to the Bulgarian Ministry of Education and Science (F-1407/2004). NM and RKP are also grateful to Bulgarian Academy of Sciences and the Royal Society (UK) for a collaborative research grant. SA's contribution was supported by NSF Grants AST-0071260 and 0507381 to The Citadel.

References

- Aerts, C., De Cat, P., Peeters, E. et al. 1999, A&A 343, 872
 Asplund, M., Grevesse, N., Sauval, A. J. 2005, in ASP Conf. Ser. 336: Cosmic Abundances as Records of Stellar Evolution and Nucleosynthesis, eds. T.G. Barnes & F. N. Bash, 25
 Azzopardi, M. 1981, Structure and Distance Modulus of the SMC from Blue Supergiants. In: D'Odorico S., Baade D., Kjar K. (eds.) Proceedings of the ESO Workshop on The most massive stars", Garching, p. 227
 Burki, G. 1978, A&A, 65, 357
 Bychkov, V. D., Bychkova, L. V., Madej, J. 2003, A&A 407, 631
 Cassinelli, J. P. & Macgregor, K. B. 2000, ASP Conf. Ser. 214, in The Be phenomenon in early-type stars, 337
 Crowther, P. A., Lennon, D. J., Walborn, N. R. 2006, A&A 446, 279
 Fitzpatrick, E. L., Garmany, C. D. 1990, ApJ 363, 119
 Fullerton, A., Gies, D. R., Bolton, C. T. 1996, ApJS 103, 475
 van Genderen, A. M. 2001, A&A 366, 508
 Grevesse, N., Sauval, A. J. 1998, SSRv 85, 161
 Henrichs, H. F. 2001, ASP Conf. Ser. 248, 393
 Hillier, D. J., Miller, D. L. 1998, ApJ 496, 407
 Hoffleit, D., Jaschek, C. 1982, The Bright Star Catalogue, 4th edition (New Haven: Yale University Observatory)
 Hubeny, I. 1988, Comput. Phys. Commun. 52, 103
 Hurbig, S., Briquet, M., Scholler, M. et al. 2007, ASPC 361, 434
 Humphreys, R. 1978, ApJS 38, 309
 Humphreys, R., McElroy, D. B. 1984, ApJ 284, 565
 Israelian, G., Chentsov, E. & Musaev, E. 1997, MNRAS 290, 521
 Kaufer, A., Stahl, O., Wolf, B. et al. 1996, A&A 305, 887
 Kaufer, A., Stahl, O., Wolf, B. et al. 1996, A&A 314, 599
 Kaufer, A., Stahl, O., Wolf, B. et al. 1997, A&A 320, 237
 Kaufer, A., Stahl, O., Prinja, R. et al. 2006, A&A 447, 325
 Kudritzki, R.-P. 1980, A&A 85, 174
 Markova, N. & Valchev, T. 2000, A&A 363, 995
 Markova, N., Puls, J. 2008, A&A 478, 823
 Markova, N., Puls, J., Repolust, T. et al. 2004, A&A 413, 693
 Markova, N., Puls, J., Scuderi, S. et al. 2005, A&A 440, 1133
 Martins, F., Schaerer, D., Hillier, D. J. 2005, A&A, 436, 1049
 Mathias, P., Aerts, C., Briquet, M. et al. 2001, A&A 379, 905
 Meynet, G., Maeder, A. 2000, A&A 361, 101
 Morel, T., Marchenko, S. V., Pati, A. K. et al. 2004, MNRAS 351, 552
 Owocki, S., un-Douls, A. 2003, ASP Conf. Ser. 305, 350
 Percy, J., Palaniappan, R., Seneviratne, R. et al. 2008, PASP 120, 311
 Petrenz, P. & Puls, J. 1996, A&A 312, 195
 Przybilla, N., Butler, K., Becker, S. R., et al. 2006, A&A 445, 1099
 Puls, J., Urbaneja, M. A., Venero, R. et al. 2005, A&A 435, 669
 Puls, J., Markova, N., Scuderi, S. et al. 2006, A&A 454, 625
 Reid, A. H. N., Bolton, C. T., Crowe, R. A. et al. 1993, ApJ 417, 320
 Roberts, D. H., Lehar, J., Dreher, J. W. 1987, AJ 93, 968
 Schaller, G., Schaerer, D., Meynet, G. et al. 1992, A&ASS 96, 269
 Schmidt-Kalet, Th. 1982, In: Landolt-Bornstein, Neue Serie, Gruppe VI, Vol. 2b, Springer, p.455
 Searle, S. C., Prinja, R. K., Massa, D. et al. 2008, A&A, 481, 777

⁹ (Depending on the size of the $H\alpha$ forming region emission may not appear in the spectrum.)

¹⁰ Given that only one spectral line has been used for these measurements an error of 20 Gauss seems somewhat unrealistic and likely represents only a lower limit.

- Severny, A. 1970, ApJ 159, L73
Simon-Diaz, S., Herrero, A. 2007, A&A 468, 1063
Townsend, R. H. D., 2007, AIPC, 948, 345
Trundle, C., Lennon, D. J. 2005, A&A 434, 677
Vink, J.S., de Koter, A., Lamers, H.J.G.L.M. 2000, A&A 362, 295
ud Doula, A., Owocki, S., Townsend, R. H. D., 2008, MNRAS, accepted (arXiv0712.2780)
Waelkens, C., Aerts, C., Kestens, E. et al. 1998, A&A 330, 215
natbib